

Photodetachment of H^- and Li^-

E. Lindroth*

Department of Atomic Physics, Stockholm University, S-104 05 Stockholm, Sweden

(Received 7 April 1995)

The photodetachment cross sections for H^- and Li^- in the vicinity of the $H(n=2-4)$ and $Li(n=3-4)$ thresholds are calculated. A discrete numerical basis set, combined with the method of complex rotation, is used to construct highly correlated descriptions of both initial and final states. The energies and widths of the doubly excited states are calculated directly and compared with results from experiments and other calculations when available. Other resonance parameters for photoexcitation from the ground state to the autodetaching states, describing the shape and the strength of the resonances, are also calculated. Mass polarization was considered for the doubly excited states of H^- , but was found to be much smaller than the present experimental accuracy. The possibility of describing a photodetachment resonance with a Fano profile, i.e., with a few resonance parameters connected to properties of a specific autodetaching state, is investigated and it is concluded that most resonances in Li^- in the region studied, where overlapping resonances are common, cannot be meaningfully analyzed in this way.

PACS number(s): 31.15.Ar, 31.50.+w, 32.80.Gc, 32.80.Dz

I. INTRODUCTION

Negative ions are known to be very sensitive to electron correlation. This is especially true for doubly excited states where the interaction between the two electrons in the outer pair is often comparable in strength to the interaction of each electron with the core. The motion of the excited electrons then becomes highly correlated and excited negative ions thus constitute prototype systems for studies of correlation.

Most experimental and theoretical investigations of double excitation in negative ions involve the simplest example, the H^- ion. Experimental studies of photo double excitation and detachment in H^- have been reported by Bryant and co-workers [1-5]. H^- has also been an attractive target for theoretical efforts and several computational techniques have been applied; see Ref. [6] and references therein. The more recent investigations include the highly accurate calculations of energies and widths for certain states by Ho [7] and by Ho and Bhatia [8], who combine Hylleraas wave functions with the use of complex rotation. Other recent calculations have been performed by Tang *et al.* [9], who use a close-coupling method in terms of hyperspherical coordinates, and by Sadeghpour *et al.* [10] who use the R -matrix method.

The first observation of resonance structure in Li^- was reported recently by Berzinsh *et al.* [11]. The energy region studied was between the $Li(3s)$ and $Li(3p)$ thresholds and the observed resonances were shown to be well explained by a calculation based on the method of complex rotation which accounted for full correlation between the outer electrons. The computational method used in Ref. [11] is here applied to H^- around the $H(n=2-4)$ thresholds and to Li^- around the $Li(n=3-4)$ thresholds. The method is described in more detail in Sec. II.

Li^- is in some sense the second simplest negative ion. The main difference compared to H^- is that the nuclear core is replaced by a more extended core consisting also of the

two $1s$ electrons. Notable is that in spite of the fact that Li^- has a particularly simple extended core it has a profound effect on the resonance structure. The energy positions (relative to the double detachment limit) do not change very much, but the lifting of the degeneracy of different ℓ states with the same n quantum number opens up new decay channels and the widths increase dramatically. The only previous theoretical studies of photodetachment in Li^- are with the R -matrix method. Pan *et al.* in Ref. [12] have calculated the cross section below the $Li(n=5)$ and $Li(n=6)$ thresholds and in Refs. [13,14] the region around $Li(n=3)$ was investigated, where the result was in good agreement with Ref. [11].

Experimental data for photodetachment resonances are often fitted to some version of the Fano analytical line shape in order to deduce the width and the energy position of a certain autodetaching state. This is a meaningful approach for H^- where the resonances are well separated. In Li^- , however, broad and overlapping resonances are common and there is no longer a one to one correspondence between a certain doubly excited state and a cross section resonance. This is investigated here and it is concluded that most resonances in Li^- in the studied region cannot be meaningfully analyzed with a small number of resonance parameters. This is particularly striking in the region around the $Li(3p)$ threshold, but it is also observed in the vicinity of the $Li(n=4)$ thresholds where a fit to a Fano profile gives somewhat meaningless results. The approximations which link the method used here with the Fano type of cross section profile are described in Sec. II A and this aspect of the results is discussed in Sec. III C.

II. THEORY

The present calculation exploits a recently developed approach [15] which combines complex rotation with the use of a discrete numerical basis set [16]. It is shown in Ref. [16] how a discrete numerical basis set can be obtained if the atom is placed in a spherical box and the one-particle Schrödinger equation is discretized on a lattice to give a matrix

*Electronic address: lindroth@atom.msi.se

equation. The eigenvectors of the symmetric matrix constitute a basis set which is complete on the chosen lattice. A choice of an N -point lattice gives N orthogonal basis set functions. Only the eigenstates with negative eigenvalues correspond to physical states. The eigenstates with positive eigenvalues constitute a pseudocontinuum with which the physical states can be described. The generalization to complex coordinates was discussed in Ref. [15]. The method of complex rotation, where the radial coordinates are scaled with a complex constant, $r \rightarrow r e^{i\theta}$, has been used extensively to account for the instability of autoionizing states; see, e.g., Refs. [17–20,7]. In Ref. [15] perturbation theory to all orders was used to account for full correlation between the two electrons in doubly excited helium. Later cross sections for dielectronic recombination into such states were also calculated [21]. Here perturbation theory is used to calculate the ground states of H^- and Li^- , while a discretized representation of the spectrum of final states was obtained by diagonalization of the matrix for the interaction between the two outer electrons. This gives a set of two-particle basis functions which again is complete on the chosen grid. Some of these states correspond to rather localized physical states which can be well described on the grid and in the spherical box. The other states constitute a discretized description of states where at least one electron is in the continuum. This two-particle pseudocontinuum does not correspond to physical states, but it can be used to describe the direct detachment channels after photoabsorption.

Rescigno and McKoy [22] have discussed how the method of complex rotation can be applied to photoabsorption. Following them we write the cross section as

$$\sigma(\omega) = \frac{e^2}{4\pi\epsilon_0} \frac{4\pi}{3} \frac{\omega}{c} \times \text{Im} \left(\sum_n \frac{\langle \Psi_0 | \sum_j r_j e^{i\theta} | \Psi_n \rangle \langle \Psi_n | \sum_j r_j e^{i\theta} | \Psi_0 \rangle}{E_n - E_0 - \hbar\omega} \right), \quad (1)$$

where each Ψ represents a correlated many-particle state with a complex energy, $E_n = E^r - i\Gamma/2$. The sum over final states, Ψ_n , goes over all optically allowed states, continuum states as well as doubly excited states. Equation (1) accounts thus for direct photodetachment as well as autodetachment preceded by photoexcitation to a doubly excited state. The initial ground state is denoted by Ψ_0 . The usual expression

which requires summation over discrete states, Ψ_n , and integration over continuum states is here replaced by a summation over the discretized two-electron spectrum. Due to the use of complex rotation, this sum can be carried out directly without any special considerations close to the poles in the energy denominator. Equation (1) is obtained with only a few approximations; a discretized continuum is used, the treatment is nonrelativistic, and the photon-ion interaction is considered in lowest order within the dipole approximation. When experimental photodetachment data are analyzed, however, they are often fitted to an approximate expression for the cross section consisting of a simple background (e.g., constant or linearly dependent on ω) plus a Fano profile [23]:

$$\sigma(\omega) = \sigma_0 \frac{(q + \varepsilon)^2}{1 + \varepsilon^2} \quad (2)$$

where

$$\varepsilon = \frac{\hbar\omega - (E^r - E_0)}{\Gamma/2}. \quad (3)$$

The Fano expression implies that the deviation from the simple background can be described by three resonance parameters; the resonant energy $E^r - E_0$, the width Γ , and the shape parameter q of the resonant state alone. The derivation of Eq. (2) in Ref. [23] assumes an isolated state embedded in a continuum. We will here call this *the one-state approximation* and it is interesting to see how this approximation is linked to Eq. (1).

A. Connection to the Fano approximation

A general doubly excited state is embedded in the continuum. This is accounted for when the wave function is constructed in the scheme of complex rotation and the complex energy is then $E^r - i\Gamma/2$. The cross section is obtained according to Eq. (1) as a sum over contributions from all possible final states. As Fano did in Ref. [23] we consider now a doubly excited state, k , and assume that for photon energies close to $(E_k^r - E_0)$ the shape of the cross section is predominantly given by the state k , the resonant state, alone. Nonresonant states are assumed to contribute to a simple background only. The contribution from the state k is obtained from Eq. (1) as

$$\begin{aligned} \sigma_k(\omega) &= \frac{e^2}{4\pi\epsilon_0} \frac{4\pi}{3} \frac{\omega}{c} \text{Im} \left(\frac{\langle \Psi_0 | \sum_j r_j e^{i\theta} | \Psi_k \rangle \langle \Psi_k | \sum_j r_j e^{i\theta} | \Psi_0 \rangle}{E_k - E_0 - \hbar\omega} \right) \\ &= C \hbar\omega \text{Im} \left\{ \frac{R_k + iI_k}{(E_k^r - E_0 - \hbar\omega) - i\Gamma_k/2} \right\} \\ &= C \hbar\omega \left\{ \frac{R_k \Gamma_k/2}{(E_k^r - E_0 - \hbar\omega)^2 + \Gamma_k^2/4} + \frac{(E_k^r - E_0 - \hbar\omega) I_k}{(E_k^r - E_0 - \hbar\omega)^2 + \Gamma_k^2/4} \right\} \end{aligned} \quad (4)$$

where C , a dimensionless constant,

$$C = \frac{e^2}{4\pi\epsilon_0} \frac{4\pi}{3} \frac{1}{\hbar c}, \quad (5)$$

and R and I , the real and imaginary parts of the squared matrix element,

$$R_k = \text{Re} \left\{ \left\langle \Psi_0 \left| \sum_j r_j e^{i\theta} \right| \Psi_k \right\rangle \left\langle \Psi_k \left| \sum_j r_j e^{i\theta} \right| \Psi_0 \right\rangle \right\}, \quad (6)$$

$$I_k = \text{Im} \left\{ \left\langle \Psi_0 \left| \sum_j r_j e^{i\theta} \right| \Psi_k \right\rangle \left\langle \Psi_k \left| \sum_j r_j e^{i\theta} \right| \Psi_0 \right\rangle \right\}, \quad (7)$$

have been introduced. If, further, ϵ , as defined in Eq. (3), is introduced the resonant part of the cross section, Eq. (4), can be rewritten as

$$\sigma_k(\omega) = \frac{CI_k}{1+\epsilon^2} \left\{ \epsilon + \frac{E_k^r - E_0}{\Gamma_k/2} \right\} \left\{ \frac{R_k}{I_k} - \epsilon \right\}. \quad (8)$$

In order to see the relation between Eq. (8) and the Fano expression in Eq. (2) σ_k is shifted with a constant σ_k^{min} , its smallest value. After the minimum of Eq. (8) is found and subtracted it is, after a substantial amount of algebra, possible to write $\sigma_k(\omega) - \sigma_k^{\text{min}}$ as

$$\sigma_k(\omega) - \sigma_k^{\text{min}} = \sigma_0 \frac{(\epsilon + q)^2}{1 + \epsilon^2} \quad (9)$$

where

$$\sigma_0 = -\frac{I_k C}{2q} \left(\frac{E_k^r - E_0}{\Gamma_k/2} - \frac{R_k}{I_k} \right) \quad (10)$$

and

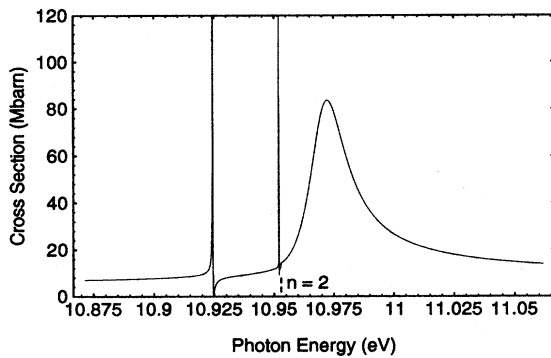


FIG. 1. Calculated total photodetachment cross section of H^- around the $H(n=2)$ threshold. The threshold at 10.9530 eV is indicated in the figure. The resonance at 10.924 eV is associated with a narrow doubly excited state dominated by $2snp$ and $2pns$ configurations in approximately equal amounts. The narrow resonance at 10.952 eV is associated with a Rydberg-like state. The broad resonance peaking at 10.972 eV is associated with a state dominated by $2snp$, $2pns$, and $2pdn$ configurations. The possibility for this state to decay to $H(n=2)$ by autodetachment explains its broader width.

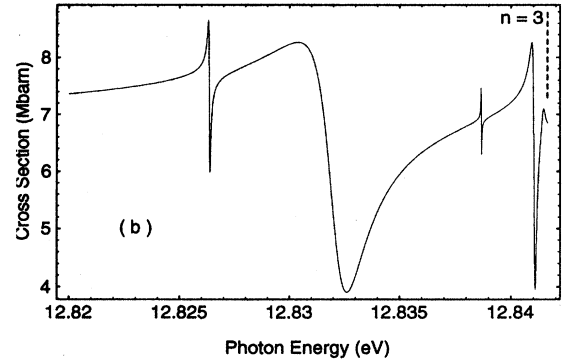
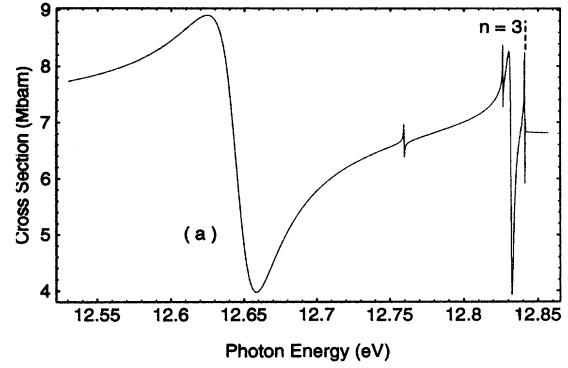


FIG. 2. Calculated total photodetachment cross section of H^- below the $H(n=3)$ threshold. The threshold is situated just after the last resonance peak, at 12.8416 eV. The states associated with the first two resonances are dominated by configurations with $n_1 = n_2 = 3$ and $n_1 = 3, n_2 = 4$. The last four resonances are all associated with states of Rydberg-like character. The threshold region is shown in more detail in (b).

$$q = b \pm \sqrt{b^2 + 1} \quad (11)$$

for $I < 0$ and $I > 0$, respectively, and

$$b = \left(\frac{(E_k^r - E_0)}{\Gamma_k/2} \frac{R_k}{I_k} + 1 \right) / \left(\frac{R_k}{I_k} - \frac{(E_k^r - E_0)}{\Gamma_k/2} \right). \quad (12)$$

According to Eq. (9) the cross section has a minimum for $\epsilon = -q$ and a maximum for $\epsilon = 1/q$. The difference between its smallest and largest values is thus

$$\Delta\sigma = \sigma_0(1 + q^2). \quad (13)$$

This value indicates the deviation from the background in, e.g., the photodetachment spectra in Figs. 1–5 and is listed as $\Delta\sigma_{\text{max}}$ in Tables I–IV. For very narrow resonances this theoretical $\Delta\sigma$ is of course larger than the observable one which will be affected by the width of the light source used to photoexcite the ion. For states with extremely narrow autodetachment width it will further be necessary to consider radiative broadening.

Equation (9) is a cross section profile of the Fano type. When resonance parameters are obtained from experimental data this is usually done by a fit to such an expression. Since the full cross section, Eq. (1), is a sum over all $\sigma_k(\omega)$ the Fano approximation relies on the assumption that the reso-

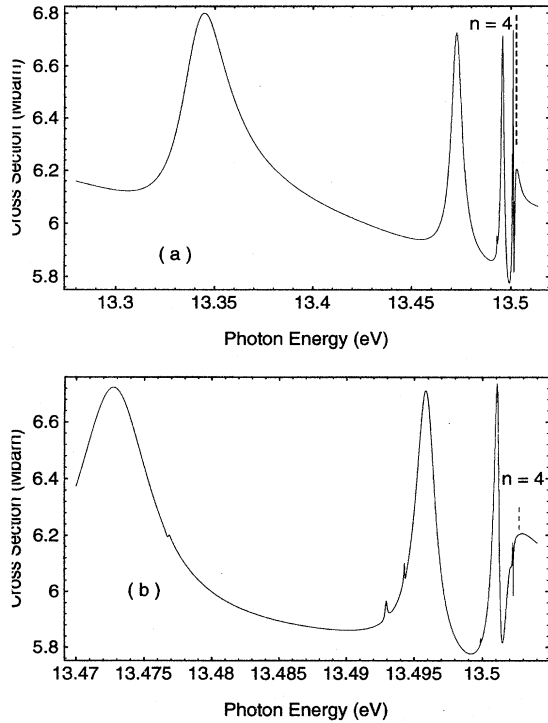


FIG. 3. Calculated total photodetachment cross section of H^- below the $H(n=4)$ threshold. The threshold is situated at 13.5027 eV. The states associated with the two first resonances are dominated by configurations with $n_1=n_2=4$ and $n_1=4, n_2=5$. The other resonances are all associated with states of Rydberg character. The threshold region is shown in more detail in (b).

nances are well separated and do not interfere with each other. Below it will be demonstrated that this approximation is valid for resonances in H^- , but that it is often insufficient in the case of Li^- .

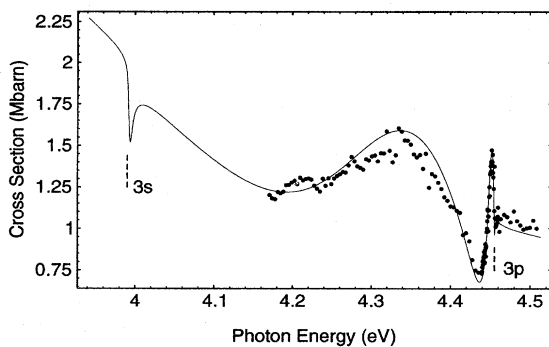


FIG. 4. Calculated total photodetachment cross section of Li^- below the $Li(3p)$ threshold. The $Li(3s)$ threshold at 3.991 eV and the $Li(3p)$ threshold at 4.452 eV are indicated in the figure. The broad resonance between the thresholds is mainly associated with a doubly excited state at 4.32 eV. This state has a width of 0.36 eV and is thus overlapping the narrow peak, associated with Rydberg-like states, just below the $Li(3p)$ threshold. Due to the overlapping resonances the cross section cannot be described by a Fano profile. The dots show the experimental result from Ref. [11].

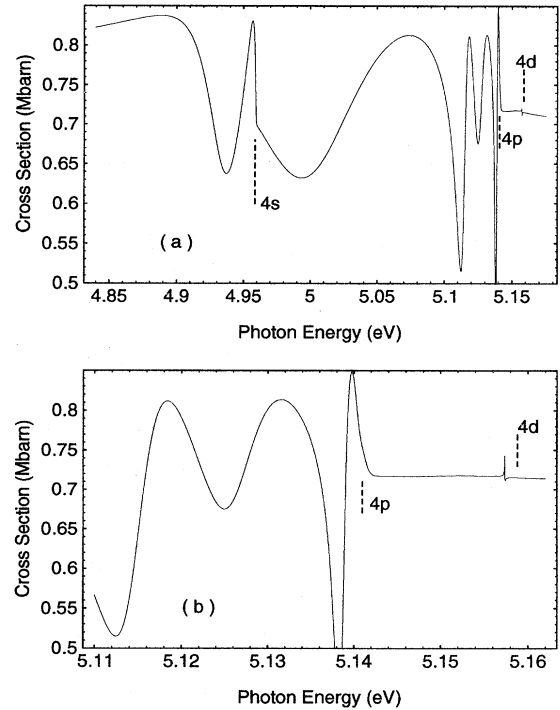


FIG. 5. Calculated total photodetachment cross section of Li^- below the $Li(4s)$, $Li(4p)$, and $Li(4d)$ thresholds. The $Li(4s)$ threshold at 4.959 eV, the $Li(4p)$ threshold at 5.141 eV, and the $Li(4d)$ threshold at 5.159 eV are all indicated in the figure. The resonance below the $Li(4s)$ threshold is associated with a state at 4.935 eV with large admixtures of $4s4p$ and $4p4d$ configurations. It is overlapping the threshold and clearly affected by that (see Fig. 7). The broad resonance between the $Li(4s)$ and the $Li(4p)$ is associated with a state which has a large admixture of the $4p4d$ configuration. The narrower resonances below the $Li(4p)$ threshold are associated with Rydberg-like states. The doubly excited states associated with the resonances in the region shown here are less overlapping compared to the states below the $Li(3p)$ threshold. Two distinguishable resonance peaks due to Rydberg-like states can thus be seen, while only one such resonance can be seen below the $Li(3p)$ threshold due to closely situated states. The small resonance at 5.157 eV is situated just below the $Li(4d)$ threshold. The threshold region is shown in more detail in (b).

B. Computational method

To obtain a representation of the final states after photoabsorption the matrix for the interaction between the two outer electrons is diagonalized. This matrix consists of elements

$$\left\langle (\psi_k \psi_l)^1 P^0 \left| \sum_{j=1}^2 h(r_j e^{i\theta}, \Omega) + \frac{1}{r_{12}} e^{-i\theta} \right| (\psi_m \psi_n)^1 P^0 \right\rangle, \quad (14)$$

where ψ are basis set orbitals, eigenstates to the one-particle Hamiltonian, h , and $e^{i\theta}$ is the complex constant with which the radial variables are scaled. For H^- h is the discretized hydrogenlike Hamiltonian. Typically 1800 different $|\psi_k \psi_l\rangle$ combinations are used, including both continuum and bound orbitals, but the selection is limited to sp , pd , df , and fg

TABLE I. Comparison between experimental and theoretical results for $^1P^o$ states of H^- around the $H(n=2)$ threshold. The peak size of the resonances is indicated in the sixth column where the calculated difference between the smallest and the largest cross section contribution from the state alone is given, cf. Eq. (13). The integrated cross section is given in the last column, cf. Eq. (16). Total energies are given in a.u. Transition energies from the ground state as well as widths are given in eV. 1 a.u. = 27.211 396 $M/(M+m)$ eV = 27.196 700 eV. The total energy of the ground state of H^- has been calculated by Drake [24] to be $-0.527\,731\,7\dots$ a.u. This value includes mass polarization and relativistic effects.

Source	E_{tot} (a.u.)	E_{tran} (eV)	Γ (eV)	q	$\Delta\sigma_{max}$ (Mb)	Strength (eV Mb)
Present ^a	-0.12605	10.924	0.000034	-17.1	≈ 2600	0.14
Ho ^b	-0.1260498		0.0000359			
Tang <i>et al.</i> ^c	-0.12606		0.000065			
Sadeghpour <i>et al.</i> ^d	-0.126014		0.0000288			
Expt. ^e		10.9264 \pm 0.0006				
Present ^a	-0.12504	10.952	<0.000002	-12.7	≈ 1900	0.006
Tang <i>et al.</i> ^c	-0.12503					
Present ^a	-0.12437	10.970 ^f	0.0185	-4.0	76	1.95
Tang <i>et al.</i> ^c	-0.12432		0.0169			
Sadeghpour <i>et al.</i> ^d	-0.124242		0.0186			
Ho and Bhatia ^g	-0.12436 \pm 3 \times 10 ⁻⁵		0.0188 \pm 2 \times 10 ⁻⁴			
Expt. ^h			0.0212 \pm 0.0011	-4.92 \pm 0.33		

^aPartial waves included up to $\ell_{max}=4$.

^bReference [20], complex rotation, partial waves included up to $\ell_{max}=4$.

^cReference [9], close-coupling method in terms of hyperspherical coordinates.

^dReference [10], R -matrix method.

^eMacArthur *et al.* [2].

^fThe peak of the resonance arising from this state is calculated to be situated at 10.972 eV.

^gReference [8], Hylleraas wave functions and complex rotation.

^hBryant *et al.* [26]. The resonance is determined in their study to be situated 0.0460 \pm 0.0004 eV above the sharp resonance at 10.924 eV, which is in perfect agreement with the present calculation.

symmetries. The number of partial waves included is the only important approximation for H^- and determines the number of digits given in Tables I–III. For Li^- approximations are also made concerning the interaction between the core and the outer electrons. The one-particle basis set used consists of orbitals obtained in the Hartree-Fock potential arising from the $1s^2$ core plus a nonlocal polarization potential, described in the Appendix, which accounts for the dominating correlation effects in neutral Li. Except for this correction the core is assumed to be inert. The eigenvectors of the matrix consisting of the elements in Eq. (14) are denoted Ψ_n and constitute a discretized description of the final states. This representation of the possible final states is used, as shown in Eq. (1), to calculate the cross section. Some of the states Ψ_n are rather localized doubly excited states and the real and imaginary parts of their complex eigenvalue E_n correspond to their energy and half-width, respectively. The other states constitute a discretized description of the bound-continuum channels. The ground states of both H^- and Li^- are calculated by perturbation theory, which makes possible an accurate description. The result for H^- , with partial waves up to $\ell_{max}=10$, is a total energy of $-0.527\,747$ a.u.,

which can be compared to the extremely accurate result for the nonrelativistic energy by Drake [24] of $-0.527\,751\,016\,544\,306(85)$ a.u. The neglect of higher partial waves is the most likely source of the discrepancy in the sixth decimal place; see Ref. [16]. For Li^- the result for the energy compared to that of the ground state of Li^+ is $E(Li^-) - E(Li^+) = -0.2214$ a.u. after inclusion of partial waves up to $\ell_{max}=8$. This can be compared to $-0.220\,461$ a.u. from a complete coupled-cluster (with single and double excitations) calculation [25]. The main reason for the discrepancy here is the approximative treatment of the core. This approximation is less severe for the excited states which have a smaller overlap with the $1s^2$ core.

Mass polarization

Since H^- is a system with a very light nucleus it cannot be assumed *a priori* that nuclear motion can be neglected when high accuracy is aimed for. Nuclear motion gives rise to two extra terms in the Hamiltonian,

TABLE II. Comparison between experimental and theoretical results for $^1P^o$ states of H^- around the $H(n=3)$ threshold. The peak size of the resonances is indicated in the sixth column where the calculated difference between the smallest and the largest cross section contribution from the state alone is given, cf. Eq. (13). The integrated cross section is given in the last column, cf. Eq. (16). Total energies are given in a.u. Transition energies from the ground state as well as widths are given in eV. 1 a.u. = 27.211 396 $M/(M+m)$ eV = 27.196 700 eV. The total energy of the ground state of H^- has been calculated by Drake [24] to be $-0.527\,731\,7\dots$ a.u. This value includes mass polarization and relativistic effects.

Source	E_{tot} (a.u.)	E_{tran} (eV)	Γ (eV)	q	$\Delta\sigma_{max}$ (Mb)	Strength (eV Mb)
Present ^a	-0.06273	12.647 ^c	0.0326	-0.74	4.9	0.075
Tang <i>et al.</i> ^c	-0.06272		0.0326			
Sadeghpour <i>et al.</i> ^d	-0.062695		0.0334			
Ho ^e	-0.06271675		0.03240			
Expt. ^f		12.650 ± 0.004	0.0275 ± 0.0008	-0.81 ± 0.02		
Expt. ^g		12.650 ± 0.001	0.0390 ± 0.002	-0.716 ± 0.37		
Expt. ^h		12.652 ± 0.003	0.030 ± 0.003			
Present ^a	-0.05857	12.760	0.00024	-1.26	0.8	7×10^{-5}
Tang <i>et al.</i> ^c	-0.05859		0.000261			
Sadeghpour <i>et al.</i> ^d	-0.058866		0.000402			
Ho ^e	-0.0585718		0.0002444			
Present ^a	-0.05612	12.826	0.00006	-0.74	2.7	7×10^{-5}
Tang <i>et al.</i> ^c	-0.05614					
Ho ^e	-0.0561167		0.000057			
Present ^a	-0.05590	12.832 ⁱ	0.00193	-0.57	4.4	0.007
Tang <i>et al.</i> ^c	-0.05591		0.00155			
Sadeghpour <i>et al.</i> ^b	-0.055832		0.00116			
Ho ^e	-0.055907		0.0019			
Expt. ^f		12.837 ± 0.004	0.0016 ± 0.0003	-0.67 ± 0.14		
Present ^a	-0.05566	12.839	0.00001	-1.0	1.3	5×10^{-7}
Present ^a	-0.05558	12.841	0.0001	-0.59	4.4	0.0004

^aPartial waves included up to $\ell_{max} = 4$.

^bThe peak of the resonance arising from this state is calculated to be situated at 12.624 eV.

^cReference [9], close-coupling method in terms of hyperspherical coordinates.

^dReference [10], R -matrix method.

^eReference [7], Hylleraas wave functions and complex rotation.

^fHamm *et al.* [1].

^gCohen *et al.* [3].

^hHalka *et al.* [5].

ⁱThe peak of the resonance arising from this state is calculated to be situated at 12.830 eV.

TABLE III. Comparison between experimental and theoretical results for $^1P^o$ states of H^- below the $H(n=4)$ threshold. The peak size of a resonance associated with a certain state is indicated in the sixth column where the calculated difference between the cross section maximum and minimum from this state alone is given, cf. Eq. (13). The integrated cross section is given in the last column, cf. Eq. (16). Total energies are given in a.u. Transition energies from the ground state as well as widths are given in eV. 1 a.u. = 27.211 396 $M/(M+m)$ eV = 27.196 700 eV. The total energy of the ground state of H^- has been calculated by Drake [24] to be $-0.527\ 731\ 7\dots$ a.u. This value includes mass polarization and relativistic effects.

Source	E_{tot} (a.u.)	E_{tran} (eV)	Γ (eV)	q	$\Delta\sigma_{max}$ (Mb)	Strength (eV Mb)
Present ^a	-0.03718	13.341 ^b	0.0280	3.94	0.8	0.03
Tang <i>et al.</i> ^c	-0.03717		0.0280			
Sadeghpour <i>et al.</i> ^d	-0.03718		0.0283			
Ho ^e	-0.03717945		0.0281097			
Expt. ^f		13.338 ± 0.004				
Present ^a	-0.03430	13.420	0.00050	4.46	0.002	2×10^{-6}
Tang <i>et al.</i> ^c	-0.03432		0.000479			
Sadeghpour <i>et al.</i> ^d	-0.034388		0.000726			
Ho ^e	-0.0342940		0.000498			
Present ^a	-0.03235	13.473	0.0065	72.4	0.9	0.009
Tang <i>et al.</i> ^c	-0.03228		0.00407			
Ho ^e	-0.032353		0.006638			
Present ^a	-0.03220	13.477	0.00021	0.90	0.02	8×10^{-7}
Ho ^e	-0.032198		0.000209			
Present ^a	-0.03161	13.493	0.00018	16.4	0.07	2×10^{-5}
Ho ^e	-0.031613		0.000162			
Present ^a	-0.03156	13.494	0.00006	-2.35	0.07	4×10^{-6}
Ho ^e	-0.031562		0.000086			
Present ^a	-0.03150	13.496	0.0017	-19.5	0.9	0.003
Ho ^e	-0.031497		0.001760			
Present ^a	-0.03131	13.501	0.00042	-2.3	1	0.0005
Ho ^e	-0.03131		0.00339			

^aPartial waves included up to $\ell_{max}=4$.

^bThe peak of the resonance arising from this state is calculated to be situated at 13.345 eV.

^cReference [9], close-coupling method in terms of hyperspherical coordinates.

^dReference [10], R -matrix method.

^eReference [7], Hylleraas wave functions and complex rotation.

^fHalka *et al.* [5].

$$\frac{\hbar^2}{2M} \sum_i \mathbf{p}_i^2 + \frac{\hbar^2}{2M} \sum_{i \neq j} \mathbf{p}_i \cdot \mathbf{p}_j, \quad (15)$$

where M is the nuclear mass. The first term is accounted for by the use of the reduced mass of the electron. The second term, often referred to as mass polarization, is more complicated and can only be accounted for by explicit evaluation.

For the ground state of H^- mass polarization has been calculated by Drake [24] and it is found to shift the energy by $+17.897 \times 10^{-6}$ a.u. (0.486 meV). Since mass polarization is very sensitive to correlation it is interesting to check how important it is for the highly correlated doubly excited states. In order to do this the mass polarization term in Eq. (15) was added to the Hamiltonian when it was diagonalized, i.e., to

TABLE IV. Some calculated resonance parameters for Li^- between the $\text{Li}(3s)$ and $\text{Li}(3p)$ thresholds and below the $\text{Li}(4s)$ and $\text{Li}(4p)$ thresholds. Note that the resonances are often overlapping and that the full sum in Eq. (1) has to be evaluated to obtain the photoabsorption cross sections shown in Figs. 4 and 5. The peak size of a resonance associated with a certain state is indicated in the sixth column where the calculated difference between the cross section maximum and minimum from this state alone is given, cf. Eq. (13). The peak position is given in the third column. The integrated cross section is given in the last column, cf. Eq. (16). Partial waves are included up to $\ell_{\max}=4$. Energies relative to the double detachment limit are given in a.u. Transition energies from the ground state as well as widths are given in eV. 1 a.u. = 27.211 396 $M/(M+m)$ eV = 27.209 28 eV. For the the energy of the two last electrons in the ground state of Li^- the value $-0.220\ 87$ a.u. is used, obtained from the experimental value for the electron affinity of Li^- and the ionization energy of Li as discussed in Ref. [25].

Resonance location	$E-E(\text{Li}^+(1s^2))$ (a.u.)	E_{tran} (eV)	E_{peak} (eV)	Γ (eV)	q	$\Delta\sigma_{\max}$ (Mb)	Strength (eV Mb)
Below $\text{Li}(3p)^a$	-0.06202 ^b	4.322	4.436	0.360	1.58	2.2	0.53
	-0.05720 ^c	4.453	4.460	0.020	1.56	1.6	0.02
	-0.05718 ^c	4.454	4.448	0.016	-1.32	1.2	0.008
Below $\text{Li}(4s)^d$	-0.03950	4.935	4.850	0.038	-0.23	0.28	0.015
Below $\text{Li}(4p)^e$	-0.03715	4.999	5.716 ^f	0.110	0.08	0.29	0.05
	-0.03289	5.115	5.120	0.0073	0.69	0.39	0.002
	-0.03247	5.126	5.139	0.0099	0.40	0.27	0.003

^aThe ionization energy of $\text{Li}(3p)$ with the approximation used here is 0.057 12 a.u. (expt=0.057 24 a.u.) and of $\text{Li}(3s)$ 0.074 22 a.u. (expt=0.074 19 a.u.).

^bNote that the resonance profile in Fig. 4 is very much affected by the presence of the Rydberg-like states just below the $\text{Li}(3p)$ threshold.

^cNote that these two Rydberg-like states are strongly overlapping and show up as one resonance in the spectrum.

^dThe ionization energy of $\text{Li}(4s)$ with the approximation used here is 0.038 63 a.u. (expt=0.038 62 a.u.).

^eThe ionization energy of $\text{Li}(4p)$ with the approximation used here is 0.031 93 a.u. (expt=0.031 98 a.u.).

^fThe resonance associated with this state is more easily identified in Fig. 5 from its cross section minimum at 4.995 eV.

the matrix elements in Eq. (14). It was found that mass polarization affected different states quite differently. Its effect was, e.g., nearly four times more important for the broad state above the $\text{H}(n=2)$ threshold (see Sec. III A 1 below) than for the narrow state below the threshold. However, the effect was in both cases much smaller than the present experimental uncertainty.

III. RESULTS

A. H^-

H^- has been studied by several theoretical approaches. In Tables I–III a comparison is made of energies and widths of a number of $^1P^o$ states with results obtained with a few other methods. Correlation is treated very accurately with Hylleraas wave functions by Ho [7] and by Ho and Bhatia [8]. The degree of agreement between these results and the present calculation depends usually on the number of partial waves included in the present study, as has been investigated in Ref. [15]. The agreement here is generally very good. The only exception is the width of a state just below the $\text{H}(n=4)$ threshold, the last state listed in Table III, which is here predicted to be much narrower than calculated by Ho. While Ho has concentrated on accurate calculations for certain states we have here constructed a spectrum of correlated two-particle states (see Sec. II B) to represent the possible final states after photoabsorption. In this way it is possible to calculate also the cross section for photodetachment. It is

further possible to calculate the explicit contribution to the cross section from a given state; see Sec. II A. In Tables I–IV parameters for resonances associated with certain states are listed. Columns two and three give the energy of each state and the photon energy needed to reach it from the ground state, respectively. We list further the width of the state and the shape parameter q [see Eq. (11)] which primarily depends on the radiative coupling between the initial and the final states. For easier identification of the resonances in Figs. 1–5 the peak position of the resonances in the single state approximation is given when it differs visibly from the position of the resonant energy. As a measure of the strength of the resonances the difference between the cross section maximum and minimum, as calculated in the single state approximation, Eq. (13), is listed. This number corresponds, for isolated resonances, to the deviation from the background in Figs. 1–5. An alternative measure of the strength of the resonances is the integrated cross section

$$\int_0^\infty \left\{ \sigma_0 \frac{(\varepsilon + q)^2}{1 + \varepsilon^2} - \sigma_0 \right\} d(\hbar\omega) \approx \pi \sigma_0 (q^2 - 1) \frac{\Gamma}{2}, \quad (16)$$

where σ_0 is subtracted in order to integrate the deviation from the value at infinity. This value has earlier been used as an indication of the resonance strength by Fano [23] and by Bryant *et al.* [26]. The absolute value of the integrated cross section is listed in the last column of each table.

Tang *et al.* [9] have used a close-coupling method in

terms of hyperspherical coordinates. In their method, described in Ref. [27], the phase shift is calculated and the resonance parameters for a doubly excited state are deduced from it after a fit of the delay time (obtainable from the phase shift) to a Lorentzian is made. Sadeghpour *et al.* [10] have performed an extensive R -matrix calculation of the cross section for photodetachment of H^- . Also in their work the resonance parameters are obtained from the Lorentzian profile of the delay time. The method presented here differs from these methods in that here the doubly excited states are constructed explicitly. In general the agreement between the three methods is rather good although there are differences in some cases in the results for the widths. For example, for the state 12.76 eV above the ground state in H^- listed in Table II Sadeghpour *et al.* find a width which is around 60% larger than the width from the other calculations and for the state at 10.924 eV in H^- listed in Table I Tang *et al.* [9] disagree by a factor of 2 compared to the present calculation, Ref. [20], and Ref. [10].

Tang *et al.* claim that a crucial point in the calculations of accurate cross sections is the quality of the initial state wave function and that differences in this respect could be one reason for varying results in the literature. The present calculation does not really support this view. An accurate description of the ground state is not hard to obtain with the method presented here. As explained above the total energy obtained from the ground state wave function agrees within 0.001% with the extremely accurate results of Drake [24]. An accurate description of the highly correlated doubly excited final states presents a more difficult task and the main reason for discrepancies between different methods could probably be sought for here. One example is the very narrow resonance found just below the $H(n=2)$ threshold by Tang *et al.* but not considered by Sadeghpour *et al.* The state associated with this resonance has an extremely narrow autoionization width which appears to be very sensitive to the inclusion also of high angular momenta in the partial wave expansion. While most widths just change in the third or fourth figure when orbitals of fg symmetry are included, this particular width decreased by two orders of magnitude. Because of this unstable behavior the width given in Table I of this state should be viewed as an estimation. Note that this autoionization width corresponds to a lifetime of around 0.3 ns and thus the radiative broadening of this state cannot be neglected. Also in helium there exist very narrow states where extremely accurate wave functions are needed to predict the widths correctly, as has been shown by Ho [28].

1. Around the $H(n=2)$ threshold

The calculated photodetachment spectrum around $H(n=2)$ is displayed in Fig. 1 and the resonance parameters for the three resonances are shown in Table I. The first two resonances are very sharp and situated just below the $n=2$ threshold, which is seen as a sharp step at 10.953 eV in Fig. 1. The third resonance is broad and situated above the $n=2$ threshold. The numerical basis set used for H^- consists of eigenstates to the hydrogen Hamiltonian when discretized on a lattice, i.e., physical bound states and a pseudocontinuum. The wave function for the doubly excited state is a linear combination of antisymmetrized products of such basis orbitals. It is well known that the one-particle quantum num-

bers (n_1, ℓ_1) and (n_2, ℓ_2) are not even approximately good quantum numbers for doubly excited states of negative ions. Many authors (see, e.g., Refs. [10,9]), instead classify the states according to the $n_1(K, T)_{n_2}^A$ scheme. The K and T quantum numbers were introduced by Herrick and Sinanoglu [29] and describe the angular correlation, i.e., the mixing of sp , pd , df symmetries, etc., for a given set of n_1 and n_2 . The A quantum number was suggested by Lin [30] and is an indication of the nature of the radial correlation. When a state is labeled $n_1(K, T)_{n_2}^A$ it is, however, still assumed that it is meaningful to ascribe a resonance to certain n quantum numbers, which in the present case is doubtful. The lowest resonance, at 10.924 eV is, e.g., in Ref. [9] classified as being due to a $2(1,0)_3^-$ state. However, an investigation of the amount of different configurations needed to describe this state shows that only $\approx 10\%$ of $|\Psi|^2$ comes from $2s3p$ and 10% from $2p3s$. In contrast $\approx 20\%$ comes from each of the configurations $2s4p$ and $2p4s$. A less precise, but more correct, description of the state is that its composition is $2snp$ and $2pns$ configurations in approximately equal amounts, where $n \geq 3$ and dominated by low n . The comparison with experiment [2] shows a deviation for the position of the resonance of 0.002 eV, which is outside the experimental error bar of 0.0006 eV. The situation is similar for other accurate calculations. The extremely narrow state at 10.952 eV above the ground state is a Rydberg-like state with $n_1=2$ and $n_2 \gg 2$. The resonance at 10.970 eV above the ground state (the peak position is at 10.972 eV) is associated with a state situated above the $H(n=2)$ threshold. It is much broader than the two other resonances, which is due to the additional possibility of decaying to $H(n=2)$, with which the overlap is much larger than with the $n=1$ state. The state is completely dominated by $(2snp)$, $(2pns)$, and $(2pnd)$ configurations in fairly equal amounts where n is low, $n=2-5$. The difference when compared to the sharp resonance at 10.924 eV is that here a significant contribution, $\approx 15\%$, comes from $2s2p$ and that the $2pnd$ configurations are more important. This latter resonance has been investigated experimentally in detail [26]. The calculated energy difference between this state and the sharp resonance at 10.924 eV is 0.046 eV, in good agreement with the measured value of 0.0460 ± 0.0004 eV. All theories, though, predict a width which is slightly narrower than the experimental one.

When mass polarization was taken into account the resonance at 10.924 eV was shifted by

$$\Delta E \approx 0.0007 \frac{m}{m+M} \text{ a.u.} \quad (17)$$

which amounts to $\approx 10 \mu\text{eV}$ if M is the proton mass. The resonance at 10.970 eV was shifted by

$$\Delta E \approx 0.0024 \frac{m}{m+M} \text{ a.u.} \quad (18)$$

which amounts to $\approx 35 \mu\text{eV}$. The finer details of the nuclear motion thus have no consequences for the comparison between theory and experiment.

2. Below the $H(n=3)$ threshold

The calculated spectrum below $H(n=3)$ is displayed in Fig. 2 and the autodetaching states are listed in Table II. The lowest energy resonance is identified with a doubly excited state that has a calculated energy of 12.647 eV (relative to the H^- ground state) and a width of 0.033 eV. The peak is situated at 12.625 eV. This resonant state is dominated by a few hydrogenic configurations: $3s3p$ (35%), $3p3d$ (31%), and $3p4d$ (11%), and it is thus quite a good approximation to describe it as a doubly excited state with both electrons in $n=3$. The next resonance is weaker and has rather large contributions from $3s4p$ ($\approx 20\%$) and $3p4s$ ($\approx 20\%$). The three last resonances listed in Table II are Rydberg-like states dominated by $3snp$ and $3pns$ (or $3pnd$ and $3dnp$) configurations with $n \geq 3$. The threshold region is showed in more detail in Fig. 2(b).

3. Below the $H(n=4)$ threshold

The calculated spectrum below $H(n=4)$ is displayed in Fig. 3 and the autodetaching states are listed in Table III. The lowest energy resonance is here identified with a doubly excited state of a similar type as was found below $n=3$. It is dominated by a few configurations where n_1 and n_2 are equal or nearly equal, $4s4p$ (23%), $4p4d$ (38%), and $4p5d$ (9%). The next resonance is very weak and can hardly be seen in Fig. 3. It is included in Table III only for comparison with the other calculations. The last six resonances are all associated with states of Rydberg character. The threshold region is shown in more detail in Fig. 3(b).

B. Li^-

1. Below the $Li(3p)$ threshold

In Fig. 4 it is seen that for Li^- a broad resonance occupies essentially the whole region between the $Li(3s)$ and $Li(3p)$ thresholds and in addition a narrow resonance is seen just below the $3p$ threshold. The experimental data from Ref. [11], normalized to the theoretical values, are shown as black dots and the agreement is good.

The present calculation predicts a resonant state of width 0.36 eV to lie 4.32 eV above the ground state of Li^- . This state appears to be analogous to the symmetrically excited state in H^- that lies 12.647 eV above the ground state. It has a very similar energy relative the double detachment limit (-0.0620 a.u. for Li^- compared to -0.0627 a.u. for H^-), but the Li^- state is approximately one order of magnitude broader. The broadening arises from the strong coupling to the $3s\epsilon p$ continuum, a continuum which is not available below $H(n=3)$ in H^- . This resonant state in Li^- is dominated by the configurations $3p3d$ and $4s3p$ and there appears to be no significant contribution to the localized part of the wave function from configurations with one electron in the $3s$ orbital, which is also in contrast to the case of H^- .

The narrow structure just below the $Li(3p)$ threshold is due to asymmetrically excited Rydberg-like states. Two important such states are listed in Table IV. As is seen in the table the widths of these states overlap each other and the peak shown in Fig. 4 is thus due to contributions from both states. The resonance parameters for each of the states listed in Table IV thus have minor physical meaning.

The resonance parameters are not very meaningful for the broad resonance either, since its width is overlapping the Rydberg-like state, as well as the $Li(3p)$ threshold and to some extent the $Li(3s)$ threshold. Here the interference results in a narrowed structure in the spectrum, especially on the high energy side, compared to that which would arise from a hypothetically isolated doubly excited state of width 0.36 eV. While the H^- intrashell resonance below $H(n=3)$ is well described by a Fano profile, this is not the case for Li^- in this region where the resonance is affected by more than one doubly excited state, as will be discussed in Sec. III C below.

Rydberg-like resonant states are apparent in the calculated spectrum of Li^- as well as H^- . In H^- these states are bound relative to $H(n=3)$ by the strong dipolar field between the two electrons. The strength of this field is due to the degeneracy of the $H(3\ell)$ states, which results in nearly equal admixtures of $3snp$ and $3pns$ (or $3pnd$ and $3dnp$) configurations in the Rydberg states. The Rydberg-like states in Li^- , however, do not have this character. They are completely dominated by $3pn\ell$ configurations, mostly $3pns$ configurations, and the dipolar field is in this case insignificant. Here the explanation for the existence of Rydberg states is much simpler. The monopole part of the electron-electron interaction is not able to screen the core completely and the residual nuclear attraction binds the states below the $Li(3p)$ threshold.

2. Below the $Li(4s)$ and the $Li(4p)$ thresholds

The cross section in this region is displayed in Fig. 5 and the resonance parameters are listed in Table IV. One resonance is visible below the $Li(4s)$ threshold, in contrast to the $Li(n=3)$ region where no resonance was situated below $Li(3s)$. This state has large admixtures of $4s4p$ and $4p4d$ configurations and is calculated to be situated 4.935 eV above the ground state, just below the $Li(4s)$ threshold at 4.959 eV.

Between the $Li(4s)$ and the $Li(4p)$ thresholds the situation is similar to that below the $Li(3p)$ threshold. The first resonance is due to a symmetrically excited state, with a large admixture of the $4p4d$ configuration, corresponding to the symmetrically excited state in H^- below $H(n=4)$. The energies are very similar, -0.03715 a.u. for Li^- and -0.03718 a.u. for H^- , but the Li^- state is five times broader due to the possibility of autodetachment to $Li(4s)$. There are also Rydberg-like states which are narrower and better separated compared to the situation below $Li(3p)$.

C. The validity of the one-state approximation

Figures 6 and 7 show how well the one-state approximation describes the resonances in H^- and Li^- . The thin solid lines are the total cross section calculated with Eq. (1). The dashed lines show the Fano profiles, Eq. (2), determined by the calculated resonance parameters E_r , Γ , q , and $\Delta\sigma_{max}$ from Table II–Table IV. For H^- below $H(n=4)$ and for Li^- below $Li(3p)$ the Fano profile has been added to a non-constant background. These backgrounds are indicated as dashed straight lines in Fig. 6(b) and Fig. 7(a).

For Li^- below the $Li(3p)$ threshold the one-state approximation is not able to explain the resonances more than

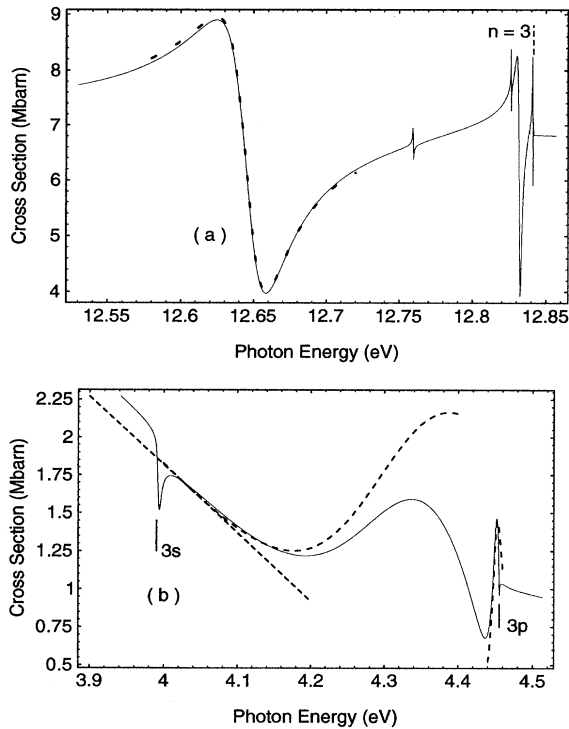


FIG. 6. These figures try to show to what extent a resonance is due to a particular doubly excited state in H^- (a) and in Li^- (b) below the $\text{H}(n=3)$ and $\text{Li}(3p)$ thresholds, respectively. The thin solid lines show the total cross section as calculated with Eq. (1). The dashed curves are Fano profiles, Eq. (2), determined by the calculated resonance parameters E_r , Γ , q , and $\Delta\sigma_{max}$ listed in Table II and Table IV. In (b) the lowest energy Fano profile is plotted on a nonconstant background which is shown as a dashed straight line. The dashed narrow peak close to the $3p$ threshold in (b) is the sum of two Fano profiles with resonance parameters from Table IV. A comparison between (a) and (b) shows that while the one-state approximation reproduces the resonance in H^- very well it clearly has difficulties in achieving more than a qualitative explanation of the resonances in Li^- .

qualitatively. In Fig. 6(b) it can be seen how the first valley of the broad resonance agrees with the Fano profile due to the doubly excited state listed on the first line in Table IV. Closer to the $3p$ threshold, however, it is hard to find any resemblance. It is clear that the sudden decrease in the cross section, starting around photon energies of 4.34 eV, is due to the presence of the Rydberg-like states just below the $3p$ threshold. The clear signature of these Rydberg-like states is the narrow peak seen in Fig. 6(b). The dashed line, which agrees reasonably well with this peak, is the *sum* of the Fano profiles due to the two states on the second and third lines of Table IV.

Below the $\text{Li}(4s)$ and $\text{Li}(4p)$ thresholds the one-state approximation explains the resonances somewhat better. It is clearly seen in Fig. 7(b) that the dip below the $\text{Li}(4s)$ threshold is due to the state 4.935 eV above the ground state. This state has a width of 0.038 eV and is thus overlapping the threshold at 4.959 eV. That the presence of the threshold is affecting the resonance is evident from Fig. 7(b). Another

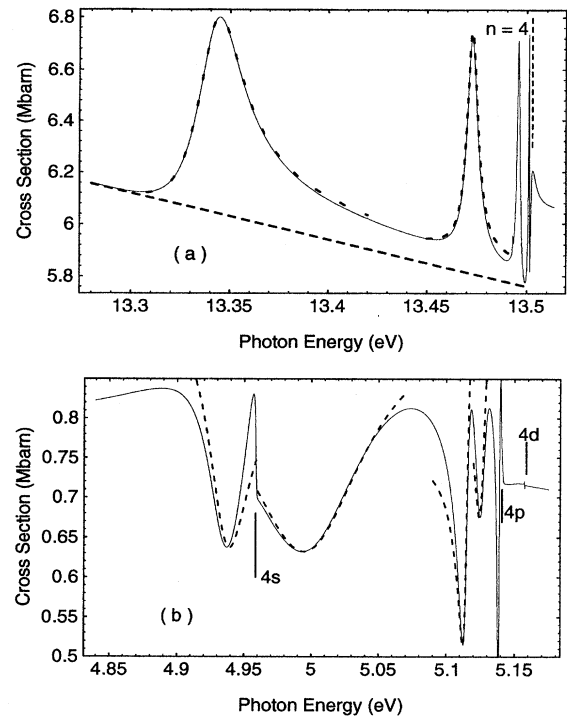


FIG. 7. These figures try to show to what extent a resonance is due to a particular doubly excited state in H^- (a) and in Li^- (b) below the $\text{H}(n=4)$ and $\text{Li}(4p)$ thresholds, respectively. The thin solid lines show the total cross section as calculated with Eq. (1). The dashed curves are Fano profiles, Eq. (2), determined by the calculated resonance parameters E_r , Γ , q , and $\Delta\sigma_{max}$ listed in Table III and Table IV. In (a) the Fano profiles are plotted on a nonconstant background which is shown as a dashed straight line. As can be seen by comparison with Fig. 6(b) the resonances in Li^- below $\text{Li}(4p)$ are somewhat better described by the one-state approximation than was possible below $\text{Li}(3p)$. Still, however, the close lying resonances will make the outcome of any attempt to fit the solid line to Fano profiles very sensitive to the energy region included in the fit.

measure of the validity of the one-state approximation is to try to fit the full cross section, the thin solid line, to a Fano profile and see how stable this fit is to the included energy region, and further to compare the resonance parameters obtained from the fit with the directly calculated parameters. For the state below the $\text{Li}(4s)$ threshold the fit results in a correct resonant energy (within 0.1%), but the width is overestimated by 50%. It is further seen in Fig. 7(b) that the resonance between the $\text{Li}(4s)$ and $\text{Li}(4p)$ thresholds is due to the state 4.999 eV above the ground state. However, the agreement between the one-state approximation and the full cross section is for a limited energy region only. The result from a fit of the full cross section to a Fano profile will then be sensitive to the region included in the fit. When the calculated cross section was fitted to a Fano profile in the region between photon energies of 4.96 eV and 5.04 eV the position and the width of the associated state were rather well reproduced (within 0.1% and 3%, respectively), but a twice as large q value indicates a more complicated background than

can be incorporated with simple Fano theory.

IV. CONCLUSIONS

It has been shown that the method of complex rotation combined with the use of a discrete numerical basis set can be used to accurately describe doubly excited states of negative ions as well as photodetachment.

The possibility of describing a photodetachment resonance with a Fano profile, i.e., with a few resonance parameters connected to properties of a specific autodetaching state, has been investigated and it was concluded that most resonances in Li^- in the studied region, where overlapping resonances are common, cannot be meaningfully analyzed in this way. This means that knowledge about the doubly excited states is not easily obtainable from the photodetachment cross section.

Mass polarization was considered for doubly excited states of H^- , but its contribution was found to be outside the present experimental accuracy.

ACKNOWLEDGMENTS

Professor D. Pegg and Dr. D. Hanstorp are gratefully thanked for fruitful discussions. G. Haeffler is thanked for assistance with the fit to Fano profiles. Financial support was received from the Swedish Natural Science Research Council (NFR).

APPENDIX

The polarization potential used for Li^- can be understood as follows. When a valence orbital, or an excited state, is solved for in the Hartree-Fock potential from the $1s^2$ core one effect that is neglected is that the presence of the outer electron affects the core and the adjustment of the core af-

TABLE V. Ionization energies of some states of Li obtained with the dipole potential, Eq. (A3), compared to Hartree-Fock results and experimental values. All results are in a.u. $1 \text{ a.u.} = 27.211396 M/(M+m) \text{ eV} = 27.20928 \text{ eV}$.

State	Hartree-Fock potential (v_{HF})	$v_{\text{HF}} + v_{\text{dipole}}$	Expt. ^a
2s	0.19630	0.19836	0.19816
2p	0.12864	0.12988	0.13024
3s	0.07380	0.07422	0.07419
3p	0.05677	0.05712	0.05724
3d	0.05556	0.05560	0.05561
4s	0.03848	0.03863	0.03862
4p	0.03178	0.03193	0.03198
4d	0.031254	0.031273	0.031276

^aC. E. Moore, *Atomic Energy Levels*, Natl. Bur. Stand. (U.S.) Circ. No. 467 (U.S. GPO, Washington, DC, 1949), Vol. I.

fects the binding energy of the outer electron. This can be accounted for by a class of diagrams transforming the Hartree-Fock orbitals to Brueckner orbitals [31,32]. The most important of these corrections, the core-valence direct contribution, is given in lowest order by the expression

$$\delta E = \sum_{rs}^{exc} \sum_a^{core} \frac{\left\langle oa \left| \frac{e^2}{4\pi\epsilon_0 r_{12}} \right| rs \right\rangle \left\langle rs \left| \frac{e^2}{4\pi\epsilon_0 r_{12}} \right| oa \right\rangle}{\epsilon_o + \epsilon_a - \epsilon_r - \epsilon_s}, \quad (\text{A1})$$

where $|o\rangle$ denotes the outer electron. The correction to the orbital can be constructed through the equation [31]

$$[\epsilon_o - h(1)]|\delta o\rangle = \sum_n^{n \neq o} \sum_{rs}^{exc} \sum_a^{core} \frac{|n\rangle \left\langle na \left| \frac{e^2}{4\pi\epsilon_0 r_{12}} \right| rs \right\rangle \left\langle rs \left| \frac{e^2}{4\pi\epsilon_0 r_{12}} \right| oa \right\rangle}{(\epsilon_o + \epsilon_a - \epsilon_r - \epsilon_s)}. \quad (\text{A2})$$

The most important term is usually due to the dipolar term in the partial wave expansion of $1/r_{12}$. Conventionally Brueckner effects are included for considered valence orbitals through the perturbation expansion. To account also for the effect on excited states we have here chosen to construct a potential which will generate the dominating part. To construct such a potential is not trivial and a complete treatment of Brueckner effects is not possible in that way. However, with a few approximations a nonlocal potential can be constructed which leaves only smaller terms to be accounted for, if desired, by perturbation theory. The first approximation concerns the energy denominator where the presence of ϵ_o makes the right-hand side of Eq. (A2) different for each orbital $|o\rangle$. We have here chosen to use $\epsilon_o = 0$. For valence

orbitals, or modestly excited states, this is a reasonable approximation since the energy denominator is dominated by the core orbital energy ϵ_a . For highly excited states the correction $|\delta o\rangle$ will be very small due to the small radial overlap between the excited state and the core and thus an accurate description is not needed. If $|o\rangle$ was a core orbital the approximation would be too crude, but we have chosen not to account for the Brueckner corrections to the core in this way. The second approximation is to restrict the partial wave expansion of $1/r_{12}$ to the dipole term, which usually dominates, and to include only the direct contribution, i.e., the one given in Eq. (A2). The potential is projected onto noncore states in order to restrict its action to valence and excited states. We get then

$$v_{dipole} = \sum_{nmrs}^{exc} \sum_a^{core} \frac{\left| n \right\rangle \left\langle na \left| \frac{e^2}{4\pi\epsilon_0} \left(\frac{1}{r_{12}} \right)_{k=1} \right| rs \right\rangle \left\langle rs \left| \frac{e^2}{4\pi\epsilon_0} \left(\frac{1}{r_{12}} \right)_{k=1} \right| ma \right\rangle \left\langle m \right|}{(\epsilon_a - \epsilon_r - \epsilon_s)}, \quad (A3)$$

where $k=1$ denotes that only the dipole term is considered. When the projection is done as in Eq. (A3) the Hermiticity of the potential is preserved. The closure relation can be used to avoid the sum over all excited states for m and n . The one-particle Hamiltonian can now be written

$$h = h_{nuc} + v_{HF} + v_{dipole}, \quad (A4)$$

where

$$v_{HF}|o\rangle = \sum_a^{core} \left\langle a \left| \frac{e^2}{4\pi\epsilon_0} \frac{1}{r_{12}} \right| ao \right\rangle - \left\langle a \left| \frac{e^2}{4\pi\epsilon_0} \frac{1}{r_{12}} \right| oa \right\rangle. \quad (A5)$$

As a measure of the improvement obtained in this way consider the ionization energy of $Li(1s^2 2s)$. The Hartree-Fock value is 0.196 30 a.u. The inclusion of the polarization potential, Eq. (21), changes it to 0.198 36, which is closer to the experimental value of 0.198 16. The results for a few excited states are listed in Table V.

-
- [1] M. E. Hamm *et al.*, Phys. Rev. Lett. **43**, 1715 (1979).
 [2] D. W. MacArthur *et al.*, Phys. Rev. A **32**, 1921 (1985).
 [3] S. Cohen *et al.*, Phys. Rev. A **36**, 4728 (1987).
 [4] P. G. Harris *et al.*, Phys. Rev. Lett. **65**, 309 (1990).
 [5] M. Halka *et al.*, Phys. Rev. A **44**, 6127 (1991).
 [6] S. J. Buckman and C. W. Clark, Rev. Mod. Phys. **66**, 539 (1994).
 [7] Y. K. Ho, Phys. Rev. A **45**, 148 (1992).
 [8] Y. K. Ho and A. K. Bhatia, Phys. Rev. A **48**, 3720 (1993).
 [9] J. Tang *et al.*, Phys. Rev. A **49**, 1021 (1994).
 [10] H. R. Sadeghpour, C. H. Greene, and M. Cavagnero, Phys. Rev. A **45**, 1587 (1992).
 [11] U. Berzinsh *et al.*, Phys. Rev. Lett. **74**, 4795 (1995).
 [12] C. Pan, A. F. Starace, and C. H. Greene, J. Phys. B **27**, L137 (1994).
 [13] C. Pan, A. F. Starace, and C. H. Greene, Bull. Am. Phys. Soc. **38**, 1124 (1993).
 [14] C. Pan, A. Starace, and C. Greene (private communication).
 [15] E. Lindroth, Phys. Rev. A **49**, 4473 (1994).
 [16] S. Salomonson and P. Öster, Phys. Rev. A **40**, 5559 (1989).
 [17] For an account of the early contributions to the complex rotation method see the whole No. 4 issue of Int. J. Quantum Chem. **14** (1978).
 [18] Y. K. Ho, Phys. Rev. A **23**, 2137 (1981).
 [19] K. T. Chung and B. F. Davis, Phys. Rev. A **26**, 3278 (1982).
 [20] Y. K. Ho, Chin. J. Phys. **29**, 327 (1991).
 [21] D. R. DeWitt *et al.*, J. Phys. B **28**, L147 (1995).
 [22] T. N. Rescigno and V. McKoy, Phys. Rev. A **12**, 522 (1975).
 [23] U. Fano, Phys. Rev. **124**, 1866 (1961).
 [24] G. W. F. Drake, Nucl. Instrum. Methods Phys. Res. Sect. B **31**, 7 (1988).
 [25] S. Salomonson and P. Öster, Phys. Rev. A **41**, 4670 (1990).
 [26] H. C. Bryant *et al.*, Phys. Rev. A **27**, 2889 (1983).
 [27] J. Tang, S. Watanabe, and M. Matsuzawa, Phys. Rev. A **46**, 2437 (1992).
 [28] Y. K. Ho, Z. Phys. D **21**, 191 (1991).
 [29] D. R. Herrick and O. Sinanoglu, Phys. Rev. A **11**, 97 (1975).
 [30] C. D. Lin, Phys. Rev. A **29**, 1019 (1984).
 [31] I. Lindgren, J. Lindgren, and A.-M. Mårtensson, Z. Phys. A **279**, 113 (1976).
 [32] I. Lindgren and J. Morrison, *Atomic Many-Body Theory, Series on Atoms and Plasmas*, 2nd ed. (Springer-Verlag, Berlin, 1986).